Measurement of triple gauge-boson couplings at 172 GeV

R. Barate, S. Jezequel, D. Buskulic, D. Decamp, P. Ghez, C. Goy, J P. Lees, A. Lucotte, M N. Minard, J Y. Nief, et al.

Measurement of Triple Gauge-Boson Couplings at 172 GeV

The ALEPH Collaboration[1]

Abstract

The triple gauge-boson couplings, $\alpha_{W\Phi}$, α_W and $\alpha_{B\Phi}$, have been measured using 34 semileptonically and 54 hadronically decaying W^+W^- candidate events. The events were selected in the data recorded during 1996 with the ALEPH detector at 172 GeV, corresponding to an integrated luminosity of 10.65 pb^{-1}. The triple gauge-boson couplings have been measured using optimal observables constructed from kinematic information of W^+W^- events. The results are in agreement with the Standard Model expectation.

---

[1]See next pages for list of authors

The ALEPH Collaboration

R. Barate, D. Buskulic, D. Decamp, P. Ghez, C. Goy, J.-P. Lees, A. Lucotte, M.-N. Minard, J.-Y. Nief,
B. Pietrzyk

  Laboratoire de Physique des Particules (LAPP), IN²P³-CNRS, 74019 Annecy-le-Vieux Cedex, France

G. Boix, M.P. Casado, M. Chmeissani, J.M. Crespo, M. Delfino, E. Fernandez, M. Fernandez-Bosman,
Ll. Garrido,[15] E. Graugès, A. Juste, M. Martinez, G. Merino, R. Miquel, Ll.M. Mir, P. Morawitz,
I.C. Park, A. Pascual, J.A. Perlas, I. Riu, F. Sanchez

  *Institut de Física d'Altes Energies, Universitat Autònoma de Barcelona, 08193 Bellaterra (Barcelona),
  Spain[7]*

A. Colaleo, D. Creanza, M. de Palma, G. Gelao, G. Iaselli, G. Maggi, M. Maggi, S. Nuzzo, A. Ranieri,
G. Raso, F. Ruggieri, G. Selvaggi, L. Silvestris, P. Tempesta, A. Tricomi,[3] G. Zito

  Dipartimento di Fisica, INFN Sezione di Bari, 70126 Bari, Italy

X. Huang, J. Lin, Q. Ouyang, T. Wang, Y. Xie, R. Xu, S. Xue, J. Zhang, L. Zhang, W. Zhao

  Institute of High-Energy Physics, Academia Sinica, Beijing, The People's Republic of China[8]

D. Abbaneo, R. Alemany, U. Becker, P. Bright-Thomas, D. Casper, M. Cattaneo, F. Cerutti, V. Ciulli,
G. Dissertori, H. Drevermann, R.W. Forty, M. Frank, F. Gianotti, R. Hagelberg, J.B. Hansen, J. Harvey,
P. Janot, B. Jost, I. Lehraus, P. Mato, A. Minten, L. Moneta,[22] A. Pacheco, J.-F. Pusztaszeri,[20]
F. Ranjard, L. Rolandi, D. Rousseau, D. Schlatter, M. Schmitt, O. Schneider, W. Tejessy, F. Teubert,
I.R. Tomalin, M. Vreeswijk, H. Wachsmuth, A. Wagner[1]

  European Laboratory for Particle Physics (CERN), 1211 Geneva 23, Switzerland

Z. Ajaltouni, F. Badaud G. Chazelle, O. Deschamps, A. Falvard, C. Ferdi, P. Gay, C. Guicheney,
P. Henrard, J. Jousset, B. Michel, S. Monteil, J-C. Montret, D. Pallin, P. Perret, F. Podlyski, J. Proriol,
P. Rosnet

  *Laboratoire de Physique Corpusculaire, Université Blaise Pascal, IN²P³-CNRS, Clermont-Ferrand,
  63177 Aubière, France*

T. Fearnley, J.D. Hansen, J.R. Hansen, P.H. Hansen, B.S. Nilsson, B. Rensch, A. Wäänänen

  Niels Bohr Institute, 2100 Copenhagen, Denmark[9]

G. Daskalakis[23], A. Kyriakis[23], C. Markou[23], E. Simopoulou, A. Vayaki[23]

  Nuclear Research Center Demokritos (NRCD), Athens, Greece

A. Blondel, J.-C. Brient, F. Machefert, A. Rougé, M. Rumpf, A. Valassi,[6] H. Videau

  *Laboratoire de Physique Nucléaire et des Hautes Energies, Ecole Polytechnique, IN²P³-CNRS, 91128
  Palaiseau Cedex, France*

T. Boccali, E. Focardi, G. Parrini, K. Zachariadou

  Dipartimento di Fisica, Università di Firenze, INFN Sezione di Firenze, 50125 Firenze, Italy

R. Cavanaugh, M. Corden, C. Georgiopoulos, T. Huehn, D.E. Jaffe

  *Supercomputer Computations Research Institute, Florida State University, Tallahassee, FL 32306-
  4052, USA [13,14]*

A. Antonelli, G. Bencivenni, G. Bologna,[4] F. Bossi, P. Campana, G. Capon, V. Chiarella, G. Felici,
P. Laurelli, G. Mannocchi,[5] F. Murtas, G.P. Murtas, L. Passalacqua, M. Pepe-Altarelli

  Laboratori Nazionali dell'INFN (LNF-INFN), 00044 Frascati, Italy

L. Curtis, S.J. Dorris, A.W. Halley, J.G. Lynch, P. Negus, V. O'Shea, C. Raine, J.M. Scarr, K. Smith,
P. Teixeira-Dias, A.S. Thompson, E. Thomson, F. Thomson, J.J. Ward

  Department of Physics and Astronomy, University of Glasgow, Glasgow G12 8QQ,United Kingdom[10]

O. Buchmüller, S. Dhamotharan, C. Geweniger, G. Graefe, P. Hanke, G. Hansper, V. Hepp, E.E. Kluge,
A. Putzer, J. Sommer, K. Tittel, S. Werner, M. Wunsch

  Institut für Hochenergiephysik, Universität Heidelberg, 69120 Heidelberg, Fed. Rep. of Germany[16]

R. Beuselinck, D.M. Binnie, W. Cameron, P.J. Dornan, M. Girone, S. Goodsir, E.B. Martin, N. Marinelli, A. Moutoussi, J. Nash, J.K. Sedgbeer, P. Spagnolo, M.D. Williams

Department of Physics, Imperial College, London SW7 2BZ, United Kingdom[10]

V.M. Ghete, P. Girtler, E. Kneringer, D. Kuhn, G. Rudolph

Institut für Experimentalphysik, Universität Innsbruck, 6020 Innsbruck, Austria[18]

A.P. Betteridge, C.K. Bowdery, P.G. Buck, P. Colrain, G. Crawford, A.J. Finch, F. Foster, G. Hughes, R.W.L. Jones, E.P. Whelan, M.I. Williams

Department of Physics, University of Lancaster, Lancaster LA1 4YB, United Kingdom[10]

I. Giehl, C. Hoffmann, K. Jakobs, K. Kleinknecht, G. Quast, B. Renk, E. Rohne, H.-G. Sander, P. van Gemmeren, C. Zeitnitz

Institut für Physik, Universität Mainz, 55099 Mainz, Fed. Rep. of Germany[16]

J.J. Aubert, C. Benchouk, A. Bonissent, G. Bujosa, J. Carr, P. Coyle, A. Ealet, D. Fouchez, O. Leroy, F. Motsch, P. Payre, M. Talby, A. Sadouki, M. Thulasidas, A. Tilquin, K. Trabelsi

Centre de Physique des Particules, Faculté des Sciences de Luminy, IN^{2}P^3-CNRS, 13288 Marseille, France

M. Aleppo, M. Antonelli, F. Ragusa

Dipartimento di Fisica, Università di Milano e INFN Sezione di Milano, 20133 Milano, Italy.

R. Berlich, W. Blum, V. Büscher, H. Dietl, G. Ganis, C. Gotzhein, H. Kroha, G. Lütjens, G. Lutz, C. Mannert, W. Männer, H.-G. Moser, R. Richter, A. Rosado-Schlosser, S. Schael, R. Settles, H. Seywerd, H. Stenzel, W. Wiedenmann, G. Wolf

Max-Planck-Institut für Physik, Werner-Heisenberg-Institut, 80805 München, Fed. Rep. of Germany[16]

J. Boucrot, O. Callot,[12] S. Chen, M. Davier, L. Duflot, J.-F. Grivaz, Ph. Heusse, A. Höcker, A. Jacholkowska, M.M. Kado, D.W. Kim,[2] F. Le Diberder, J. Lefrançois, A.-M. Lutz, M.-H. Schune, L. Serin, E. Tournefier, J.-J. Veillet, I. Videau, D. Zerwas

Laboratoire de l'Accélérateur Linéaire, Université de Paris-Sud, IN^{2}P^3-CNRS, 91405 Orsay Cedex, France

P. Azzurri, G. Bagliesi,[12] S. Bettarini, C. Bozzi, G. Calderini, R. Dell'Orso, R. Fantechi, I. Ferrante, A. Giassi, A. Gregorio, F. Ligabue, A. Lusiani, P.S. Marrocchesi, A. Messineo, F. Palla, G. Rizzo, G. Sanguinetti, A. Sciabà, G. Sguazzoni, J. Steinberger, R. Tenchini, C. Vannini, A. Venturi, P.G. Verdini

Dipartimento di Fisica dell'Università, INFN Sezione di Pisa, e Scuola Normale Superiore, 56010 Pisa, Italy

G.A. Blair, L.M. Bryant, J.T. Chambers, J. Coles, M.G. Green, T. Medcalf, P. Perrodo, J.A. Strong, J.H. von Wimmersperg-Toeller

Department of Physics, Royal Holloway & Bedford New College, University of London, Surrey TW20 OEX, United Kingdom[10]

D.R. Botterill, R.W. Clifft, T.R. Edgecock, S. Haywood, P. Maley, P.R. Norton, J.C. Thompson, A.E. Wright

Particle Physics Dept., Rutherford Appleton Laboratory, Chilton, Didcot, Oxon OX11 OQX, United Kingdom[10]

B. Bloch-Devaux, P. Colas, B. Fabbro, G. Faïf, E. Lançon, M.-C. Lemaire, E. Locci, P. Perez, H. Przysiezniak, J. Rander, J.-F. Renardy, A. Rosowsky, A. Roussarie, A. Trabelsi, B. Vallage

CEA, DAPNIA/Service de Physique des Particules, CE-Saclay, 91191 Gif-sur-Yvette Cedex, France[17]

S.N. Black, J.H. Dann, H.Y. Kim, N. Konstantinidis, A.M. Litke, M.A. McNeil, G. Taylor

Institute for Particle Physics, University of California at Santa Cruz, Santa Cruz, CA 95064, USA[19]

C.N. Booth, C.A.J. Brew, S. Cartwright, F. Combley, M.S. Kelly, M. Lehto, J. Reeve, L.F. Thompson

  Department of Physics, University of Sheffield, Sheffield S3 7RH, United Kingdom[10]

K. Affholderbach, A. Böhrer, S. Brandt, G. Cowan, J. Foss, C. Grupen, L. Smolik, F. Stephan

  Fachbereich Physik, Universität Siegen, 57068 Siegen, Fed. Rep. of Germany[16]

M. Apollonio, L. Bosisio, R. Della Marina, G. Giannini, B. Gobbo, G. Musolino

  Dipartimento di Fisica, Università di Trieste e INFN Sezione di Trieste, 34127 Trieste, Italy

J. Putz, J. Rothberg, S. Wasserbaech, R.W. Williams

  Experimental Elementary Particle Physics, University of Washington, WA 98195 Seattle, U.S.A.

S.R. Armstrong, E. Charles, P. Elmer, D.P.S. Ferguson, Y. Gao, S. González, T.C. Greening, O.J. Hayes, H. Hu, S. Jin, P.A. McNamara III, J.M. Nachtman,[21] J. Nielsen, W. Orejudos, Y.B. Pan, Y. Saadi, I.J. Scott, J. Walsh, Sau Lan Wu, X. Wu, J.M. Yamartino, G. Zobernig

  Department of Physics, University of Wisconsin, Madison, WI 53706, USA[11]

1 Introduction

All evidence for the existence of triple gauge-boson vertices and measurements of the triple gauge-boson couplings (TGCs) has, until now, been indirect or based on estimates from the Tevatron [1]. The start of LEP2 at energies above the threshold for W pair production has made it possible for the first time to study the non-Abelian gauge structure of the electroweak Standard Model directly in the clean environment of e^+e^- collisions.

Assuming the most general gauge structure of the electroweak Standard Model (SM) consistent with Lorentz invariance and $U(1)_{EM}$ gauge invariance, the ZW^+W^- and γW^+W^- vertices can be comprehensively described by 14 independent couplings [2], 7 for each vertex, which form a complete set [3].

Any theory incorporating new physics beyond the SM, while at the same time including the electroweak theory as an effective low-energy limit, may introduce small deviations in some of the general TGCs from their SM values. In this way precise measurements of the TGCs will not only establish a stringent test of the SM, but also probe for new physics in the bosonic sector. Standard Model radiative corrections also give contributions to the couplings of order one promille, comparable to the effects from, for example, SUSY theories [4].

The TGCs naturally split into three classes. Three TGCs that conserve C and P individually, one TGC that violates C and P but is CP conserving, and the remaining three TGCs describe CP violation in the triple gauge-boson sector. The large number of parameters does not allow an independent determination of all TGCs with present statistics. However, based on very general theoretical considerations it is expected to be very unlikely to observe C, P or CP violation at LEP2 [5, 6, 7]. Assuming electromagnetic gauge invariance and concentrating on the C- and P-conserving couplings reduces the number of TGCs to five: g_1^Z, κ_γ, κ_Z, λ_γ and λ_Z. The couplings related to the γW^+W^- vertex determine properties of the W, such as the magnetic dipole moment μ_W and the electric quadrupole moment q_W of the W, via

$$\mu_W = \frac{e}{2M_W}(g_1^\gamma + \kappa_\gamma + \lambda_\gamma) \tag{1}$$

$$q_W = -\frac{e}{M_W^2}(\kappa_\gamma - \lambda_\gamma).$$

In the literature the TGCs are often referred to as anomalous couplings due to their connection with the magnetic moment.

The TGCs contribute, via loop corrections, to observables which can be precisely measured at LEP1 and there has been a rich discussion on the bounds in the parameter space that can be deduced from these measurements [5, 8]. To parametrise the so-called "blind directions" in the multidimensional space of TGCs where the constraints from LEP1 analyses are very weak, three linear combination of these couplings have been proposed [2, 3, 6].

The three TGCs, $\alpha_{W\Phi}$, α_W and $\alpha_{B\Phi}$, introduced to parametrise these linear combinations, form the most general set of TGCs which can be embedded into a theory that preserves local $SU(2)_L \times U(1)_Y$ invariance. Such a requirement results in suppressing the loop corrections for observables relevant at LEP1. In terms of the notation in [3] they are

$$\alpha_{W\Phi} = \Delta g_1^Z \cos^2\theta_W$$

$$\alpha_W = \lambda_\gamma \tag{2}$$

$$\alpha_{B\Phi} = \Delta\kappa_\gamma - \Delta g_1^Z \cos^2\theta_W,$$

along with the constraints $\Delta\kappa_Z = \Delta g_1^Z - \Delta\kappa_\gamma \tan^2\theta_W$ and $\lambda_\gamma = \lambda_Z$. The Δ denotes the deviations of the respective quantity from its non-zero SM value and θ_W is the weak mixing angle. The TGCs defined in Eq. 3 differ from the TGCs measured at p$\bar{\text{p}}$ colliders, making a direct comparison of results difficult.

This analysis constrains the underlying structure of the ZW$^+$W$^-$ and γW$^+$W$^-$ vertices directly by measuring the couplings $\alpha_{W\Phi}$, α_W and $\alpha_{B\Phi}$ individually assuming the two other couplings to be fixed at zero, their SM expectation. The corresponding models for TGCs are referred to as the W$_\Phi$, W and B$_\Phi$ models, respectively [3].

The present analysis uses a data sample with $e^+e^- \to$ W$^+$W$^- \to e\nu q\bar{q}$, $\mu\nu q\bar{q}$, $q\bar{q}q\bar{q}$ candidate events. The data were recorded with the ALEPH detector at a mean centre-of-mass energy of 172.086 ± 0.060 GeV corresponding to an integrated luminosity of 10.65 pb^{-1}. The semileptonic channel $\tau\nu q\bar{q}$ and the fully leptonic channel $\ell\nu\ell\nu$ are not used in the analysis.

The paper is organised as follows. In section 2, a brief description of the ALEPH detector is given. The Monte Carlo event samples are presented together with the event selection in section 3. The kinematic reconstruction of the different decay channels are described in section 4. In Section 5, the measurements of the TGCs are presented.

2   The ALEPH Detector

In this section the ALEPH detector and its performance are briefly described. A detailed description can be found elsewhere [9, 10].

The central part of the ALEPH detector is dedicated to the reconstruction of the trajectories of charged particles. Following a charged particle from the interaction point outwards, the trajectory is measured by a two-layer silicon strip vertex detector, a cylindrical drift chamber and a large time projection chamber (TPC). The three tracking detectors are immersed in a 1.5 T axial field provided by a superconducting solenoidal coil and combined they measure high momentum charged tracks with a momentum resolution of $\sigma(1/p_T) = 6 \times 10^{-4}$ (GeV/c)$^{-1}$. Hereafter, charged particle tracks reconstructed with at least four hits in the TPC and originating from within a cylinder of length 20 cm and 2 cm radius, centred on the nominal interaction point and parallel with the beam, are denoted *good tracks*.

The electromagnetic calorimeter (ECAL) is situated between the TPC and the coil. It is a highly granular lead–proportional-wire sampling calorimeter with a total thickness of 22 radiation lengths and yields a resolution of $\delta E/E = 0.18/\sqrt{E}$, with E in GeV. Electrons are identified by their transverse and longitudinal shower profiles in ECAL and their specific ionisation in the TPC.

The iron return yoke is equipped with 23 layers of streamer tubes and forms the hadron calorimeter (HCAL). Combined with ECAL it provides a relative energy resolution of charged and neutral hadrons of $0.85/\sqrt{E}$, with E in GeV. Muons are distinguished from hadrons by their distinct pattern in HCAL and by the muon chambers composed of two layers of streamer tubes outside HCAL.

The information from the tracking detectors and the calorimeters are combined in an energy flow algorithm [10]. For each event, the algorithm provides a set of charged and neutral reconstructed particles, called energy flow objects, which are used in the analysis.

3   Event samples and selection

3.1   Monte Carlo samples

Several Monte Carlo (MC) event samples, with full detector simulation, are used in the analysis. The main reference MC sample (50000 events) is obtained using the `KORALW` [11] generator where all the TGCs are set to their SM values. In addition, MC samples with 10000 events were generated with `EXCALIBUR` [12] and `PYTHIA` [13] for systematic studies. The `KORALW` and `EXCALIBUR` samples were generated with the full set of four-fermion diagrams, whereas `PYTHIA` only provides the W^+W^- diagrams. The cross sections from `KORALW` and `EXCALIBUR` are in excellent agreement. Different W masses around the published world average, $M_W = 80.356 \text{ GeV}/c^2$, were used in the `KORALW` generation.

In addition, MC samples, each with 10000 events, were generated with non-standard anomalous TGCs in order to check the reconstruction and fitting method. These samples contain only the lowest order diagrams for W^+W^- pair production, the so-called CC03 [3] diagrams.

To check for possible systematic effects arising from colour reconnection a sample with colour reconnection was generated using `EXCALIBUR`. The model for colour reconnection assumed that strings are cylindrical space-time tubes and the reconnection probability is proportional to the space-time overlap of the string systems from the two W systems [14].

To estimate the effects from various background processes, `PYTHIA` was used to generate $q\bar{q}$ and ZZ samples. In the ZZ sample, events with final states interfering with W^+W^- final states were discarded. Two-photon processes were simulated with the `PHOT02` [15] generator. The corresponding integrated luminosity of each background sample was at least 10 times as large as that of the data.

Finally the `HERWIG` [16] generator was used to generate a $q\bar{q}$ sample, with the same integrated luminosity as the `PYTHIA` sample, for systematic studies of possible fragmentation and shape dependence of the QCD background.

3.2   Event selection

In this analysis all events are required to have at least five good tracks and a total charged energy greater than $0.10\sqrt{s}$ in order to discard low multiplicity background events.

3.2.1   Semileptonic channel

Semileptonic events are characterised by an energetic lepton and large missing energy and transverse momentum due to the undetected neutrino.

The lepton identification is based on electron and muon identification criteria using standard ALEPH methods [10]. The reconstruction of electrons incorporates final state radiation and bremsstrahlung in inactive material [17].

The missing four-momentum is used to reduce the non-radiative QCD background and remove most of the radiative component by requiring missing transverse momentum. Events with at least one lepton candidate are passed to a neural network designed to select semileptonic events using lepton track information and global event information. The output from the neural network is computed from 25 input variables. The most discriminant quantities are missing transverse and longitudinal momentum, lepton identification and number of selected leptons in the event. A complete description of all input variables can be found in Appendix A.

The neural network output for semileptonic events and background events is presented in Fig. 1a.

Events with a neural network output smaller than 0.95 are rejected. The resulting efficiency was found to be 86% with a purity of 94%. The remaining events are forced into two jets using the Durham (P scheme) jet algorithm [18], disregarding the candidate for the lepton originating from one of the W bosons. Finally, the energies of the two jets are required to be greater than 10 GeV each. After these requirements 34 semileptonic events, 14 $e\nu q\bar{q}$ and 20 $\mu\nu q\bar{q}$, are selected from data, with an expected background of 1.79 ± 0.06. The event selection and background contamination are summarised in Table 1. The main background, 1.08 events, comes from $W^+W^- \rightarrow \tau\nu q\bar{q}$ events.

3.2.2   Hadronic channel

Hadronic W^+W^- events are selected by four separated jets fully contained in the detector. The main backgrounds are rejected by requiring that the missing energy be less than 40 GeV, the number of energy-flow objects be larger than 45 and the number of jets found with the JADE [19] jet-algorithm for a $y_{\text{cut}} = 0.005$ be larger than 3. In addition each jet must contain at least 2 good tracks and the electromagnetic energy fraction in a jet is required to be less than 0.9.

The events are forced into four jets using the Durham (P scheme) jet algorithm and the resulting jets are each required to have an energy greater than 10 GeV.

To extract the W^+W^- signal with high purity and efficiency, the main selection is based on the output of another neural network. The neural network input consists of 21 variables which are chosen to optimise the selection efficiency. The most important variables to select hadronic WW events are global event quantities, followed by jet properties. A description of the variables is given in Appendix B.

The neural network output for hadronic events and background events is presented in Fig. 1b. For a cut of 0.5 on the neural network output the events are selected with an efficiency of 75% and a purity of 87%. In total 54 events pass the criteria with an expected background of 6.77 ± 0.30. The event selection and background contamination is given in Table 1.

4   Kinematic reconstruction

The important kinematic quantities for TGC measurements in W^+W^- events are the five variables:

- $\cos\theta$, the production angle of the W^-.

- $\cos\theta_{1,2}$, the polar decay angle of the charged lepton or down type quark with respect to the flight direction of the corresponding W, measured in the W rest frame.

- $\phi_{1,2}$, the azimuthal decay angle of the charged lepton or down type quark with respect to the plane defined by the direction of the corresponding W and the incoming electron.

A description of the reconstruction of the four-momenta of the W^+W^- decay products, which determine these angles, is presented in the following.

4

Table 1: *The number of events after selection for data and MC simulation in the semileptonic and hadronic channels. For the MC simulation, the contributions from different types of processes are given separately. The number of MC events is normalised to the integrated luminosity of the data.*

Channel	Semileptonic	Hadronic
data	34	54
W^+W^- MC signal	32.10	45.90
W^+W^- MC non-signal	1.08	0.20
MC QCD	0.41	6.04
MC Two-photon	0.21	0.00
MC ZZ	0.09	0.53
MC Total	33.9	52.6

4.1 Semileptonic events

In order to take into account the energy resolution of the detector combined with the loss of particles in the beam pipe or in cracks, the events are subjected to a kinematic fit using four-momentum conservation and reference mass constraints by requiring that the two decaying systems be Gaussian distributed around the W mass. The resulting four-momenta of the four reconstructed objects are used in the determination of the TGCs. The effects of initial state radiation have not been accounted for in the kinematic fit, but this does not affect the fits to the TGCs due to the fitting procedure used to extract the TGCs.

For semileptonic events the charge of the reconstructed lepton determines the W^- direction and hence allows for unambiguous determination of the primary variable for measurement of the TGCs, the production angle. Furthermore the decay angles for the leptonically decaying W system can be determined unambiguously, whereas for the hadronically decaying W the flavour of the quarks is undetermined and it is necessary to sum over the two possible four-momentum configurations. The possibility to use flavour tagging or jet-charge tagging to determine the flavour of the quarks has been studied, but with the present statistics the improvement of the bounds on TGCs was negligible.

4.2 Hadronic events

For the hadronic W^+W^- events the reconstruction of the relevant information is more complicated since there is no clean signature of the W^- direction nor any information of the particle flavours in either W systems. In this case the four jets can be paired in three different ways. To select the best pairing the kinematic fitting procedure is applied to all three pairings. The four-momenta obtained in the kinematic fit for the pairing with the lowest χ^2 value are then used in the determination of the TGCs, while the other combinations are discarded. The efficiency of the pairing is found to be 84%.

To assign a jet pair to the W^+ or W^- a jet charge algorithm is used. The charge difference between the two W systems is 2, allowing a relatively high separation efficiency. The jet charge is obtained from the pseudorapidity weighted charge of jet particles:

$$Q_{\text{jet}} = \frac{\sum_i \eta_i Q_i}{\sum_i \eta_i}, \tag{3}$$

where the sum runs over all particles assigned to the jet. The W charge is then defined

by the sum of the two jets assigned to the W, $Q_W = Q_{\text{jet1}} + Q_{\text{jet2}}$. A jet pair is then assigned to the W$^+$ based on the charge difference between the two jet pairs, ΔQ, with a probability P_+. The probability P_+ is given by

$$P_+(\Delta Q) = \frac{\mathcal{N}_+(\Delta Q)}{\mathcal{N}_+(\Delta Q) + \mathcal{N}_+(-\Delta Q)}, \tag{4}$$

where $\mathcal{N}_+$ is the distribution of the charge difference between the two W systems for true W$^+$ jet pairs obtained from MC samples. Figure 2a shows the distribution of the charge difference between the two W systems for true W$^+$ and W$^-$ decays, respectively, obtained from MC generator information. The distribution of P_+, obtained from MC simulation, is depicted in Fig. 2b. The distribution of Q_W for $P_+ < 0.5$ ($P_+ > 0.5$) is shown in Fig. 2c(d). The data is well reproduced by the MC simulation. The charge assignment efficiency for correctly paired hadronic W$^+$W$^-$ events amounts to approximately 80% for $P_+ > 0.5$.

The quark flavours are not determined which leads to a twofold ambiguity per W. Considering the W charge as undetermined implies that there is an eightfold ambiguity per hadronic event.

5   Measurement of the TGCs

Several methods to extract the anomalous couplings have been investigated in order to evaluate their sensitivity to the TGCs and study their advantages and drawbacks.

One method is a maximum likelihood fit where the event probability is evaluated from the differential cross section using the measured kinematic variables. The primary advantage of this method is that it exploits the full angular information available. However, the likelihood includes neither background nor experimental effects, resulting in a non-linear behaviour, which leads to a degradation in resolution of the TGCs.

A canonical way to account for detector smearing and acceptance is to determine the couplings by a standard five-dimensional binned likelihood fit using MC simulation. However, to bin the relevant kinematic information according to the experimental resolution would lead to a unacceptable large number of bins.

Fits to the measured $\cos\theta_W$ distribution avoid the above difficulties, but loses a considerable amount of information, especially for the semileptonic channel where the leptonic quantities give important information on the W helicity.

Instead the dimensionality can be reduced by introducing the so-called "optimal observables" (OO) which project the relevant kinematic information sensitive to a certain TGC onto a one-dimensional distribution [20]. The OO for a given TGC, α_i, is defined as the derivative of the differential cross section with respect to the coupling evaluated at the SM value

$$\text{OO}_i(\alpha_i = 0(\text{SM})) = \frac{1}{d\tilde{\sigma}(\Omega, \alpha_i)} \frac{d}{d\alpha_i}(d\tilde{\sigma}(\Omega, \alpha_i)), \tag{5}$$

where $d\tilde{\sigma}(\Omega, \alpha)$ denotes the differential cross section after folding over ambiguities. In the semileptonic case the twofold ambiguity from the hadronically decaying W is added:

$$d\tilde{\sigma}(\Omega, \alpha)_{\ell\nu q\bar{q}} = \left[\frac{d\sigma}{d\Omega_{\ell\nu j_1 j_2}} + \frac{d\sigma}{d\Omega_{\ell\nu j_2 j_1}} \right]. \tag{6}$$

In the hadronic case a summation is performed over the eightfold ambiguity, each weighted with the appropriate charge probability.

For each detected event OO_i is calculated. A maximum likelihood fit is performed to the distribution of the optimal observable using

$$\ln \mathcal{L} = \sum_{j=1}^{N} \ln P(OO_i^j, \alpha_i), \qquad (7)$$

where the probability $P(OO_i^j, \alpha_i)$ is evaluated from the distribution of OO_i obtained from MC simulation. The probability is constructed for different values of the TGCs by reweighting the MC events. The total number of observed events is included by means of a Poisson term in the likelihood function. By construction, this method is bias-free and takes into account any experimental effects, provided that the MC simulation correctly describes the data.

Fits have been performed separately in the semileptonic and hadronic channels for each of the couplings $\alpha_{W\Phi}$, α_W and $\alpha_{B\Phi}$ individually assuming the two other couplings to be fixed at zero, their SM expectation. The combined results from the analyses of the semileptonic and hadronic channels are extracted by means of fits using the sum of the log-likelihood curves from the individual channels.

5.1   Studies of Systematic Effects

The systematic uncertainties were determined, whenever possible, by modifying the MC simulation for the effect under study. In some cases it was necessary to repeat the event reconstruction, after modification, for both data and MC simulation. Unavoidably, the systematic uncertainties estimated in this way will be sensitive to statistical effects and therefore overestimated.

In the following several sources of systematic errors and their determination are briefly described.

- The analysis was repeated using MC samples generated at different values of M_W to investigate the effects due to the uncertainty in the W mass, $M_W = 80.356 \pm 0.125$ GeV [21]. The values of the measured couplings changed by typically 10% of the statistical uncertainties in the combined fits.

- The LEP energy is used in the fit to the couplings and the kinematic fitting procedure, where it enters via the constraint of four momenta conservation. Its value was varied in the range $E_{LEP} = 172.086 \pm 0.060$ GeV, which had a negligible effect on the results.

- To check for possible deviation of the calorimetric energy measurement between data and MC simulation, the hadronic part of the measured energy was varied by 4% in the MC simulation. Independently, the electromagnetic component was varied by 1.5%. The results changed by approximately 5% of the statistical uncertainties in the combined fits.

- The background from $q\bar{q}$ was changed by 5%, based on comparisons between data and MC simulation. The analysis was repeated with a $q\bar{q}$ sample generated with the HERWIG generator, which uses a different hadronisation model, to account for possible shape and fragmentation dependence in the main background. The effects on the results are below 3% of the statistical uncertainties in the combined fits.

- The background from two-photon and ZZ events was varied by 30% which resulted in negligible changes on the measured couplings.

- To investigate the effects due to the uncertainties from fragmentation and jet reconstruction, the following checks were performed.

  - The standard Durham (P scheme) algorithm was replaced by Durham (E scheme) and JADE [19] (P scheme) in both data and MC simulation. The Durham and JADE algorithms represent two conceptually different criteria for forming jets, transverse momentum and invariant mass, respectively, which are affected differently by fragmentation. The use of different jet algorithms resulted in considerable changes on the measured couplings in the hadronic channel, about 60% of the statistical uncertainty. The changes in the semileptonic channel and for the combined result were typically 20% of the statistical uncertainty.

  - For the hadronic channel, the analysis was repeated with events from the EXCALIBUR MC simulation with and without colour reconnection. The effect on the couplings was considerable for $\alpha_{W\Phi}$ where it amounted to approximately 40% of the statistical uncertainties in the combined fit.

  - The effects of Bose Einstein correlation has been investigated by repeating the analysis and weighting each MC event [22]. The weight of an event is the probability for the event having Bose Einstein correlation divided by the probability for the event having no Bose Einstein correlation. The changes in the couplings was considerable for $\alpha_{W\Phi}$ where it amounted to approximately 35% of the statistical uncertainties in the combined fit.

  - To check the effects from the uncertainties on the jet charge, the reconstructed W charge was shifted by 0.01. This number is based on comparisons between data and MC simulation (Z peak data). The changes in the couplings were about 6% of the statistical uncertainties in the combined fits.

- The effects of radiative corrections have been studied by using different event generators. The analysis was repeated using events generated with the PYTHIA generator, which uses a different approach to implement initial state radiation than KORALW. The values of the couplings changed by 10% of their statistical uncertainties. The effect of the transverse distribution of initial state radiation was estimated using the EXCALIBUR MC sample. The EXCALIBUR event generator has a different implementation of initial state radiation and generates collinear initial state radiation [23], in contrast to both KORALW and PYTHIA. The effect on the couplings was below 20% of the statistical uncertainties in the combined fits, highest for $\alpha_{W\Phi}$.

- The uncertainty due to the use of a finite number of MC events was evaluated and found to be less than 4% of the statistical uncertainties in the combined fits.

The results for the combined fits are summarised in Table 2.

The individual systematic effects are combined in quadrature, separately for positive and negative deviations from the standard values of the measured couplings. In the combined fits, the systematic uncertainties amount to 40% , 20% and 20% of the statistical uncertainties for $\alpha_{W\Phi}$, α_W and $\alpha_{B\Phi}$, respectively.

5.2 Additional checks

All the fits used in this study rely on the applicability of MC event reweighting. The validity of the reweighting procedure was checked by repeating the fits using MC samples

Table 2: *Summary of systematic uncertainties for $\alpha_{W\Phi}$, α_W and $\alpha_{B\Phi}$, for the combined fits. A description of the different sources is given in the text.*

Source	$\alpha_{W\Phi}$	α_W	$\alpha_{B\Phi}$
M_W	$-0.02/-0.04$	$+0.04/+0.02$	± 0.03
LEP Energy	$-$	$-$	$-$
Hadronic energy ($\pm 4\%$)	± 0.01	± 0.02	± 0.02
Electromagnetic energy ($\pm 1.5\%$)	$-$	± 0.03	± 0.02
Background	-0.01	-0.01	$-$
Fragmentation	$+0.09$	$+0.09/-0.16$	$+0.26$
Colour reconnection	-0.10	-0.01	$+0.10$
Bose Einstein	$+0.09$	-0.07	$+0.16$
Radiative corrections	$+0.06/-0.02$	$+0.04/-0.09$	-0.32
MC statistics	± 0.01	± 0.02	± 0.05
Total	$+0.14/-0.12$	$+0.12/-0.20$	$+0.33/-0.33$

generated with non-zero values for the TGCs. In all cases the results were in agreement within the statistical uncertainty of the MC samples.

To check the stability and the possible biases of the fitting procedure, fits were performed to several MC samples, each corresponding to the integrated luminosity of the data with statistical fluctuations. These samples, typically 200, were then reweighted to non-zero values for the TGCs and passed through the analysis chain. The *expected* 68% confidence levels, obtained from the distributions of the fit values, show good correspondence with the 68% confidence intervals obtained for data.

Finally, the stability of the analysis with respect to the event selection was tested by varying the main selection criteria within reasonable limits. The effects of all these additional checks were well below the total systematic uncertainties.

5.3 Results

In this section the results for the three TGCs, $\alpha_{W\Phi}$, α_W and $\alpha_{B\Phi}$, are presented for fits using the semileptonic and hadronic W^+W^- channels separately and combined fits. All the fits are done using a W mass of 80.356 ± 0.125 GeV/c^2, a LEP energy of $E_{LEP} = 172.086 \pm 0.060$ GeV [24] and an integrated luminosity of 10.65 ± 0.08 pb^{-1}.

While the main sensitivity to the TGCs stems from the kinematic distributions the total number of observed events also provides bounds. Figure 3 shows the total number of expected events, normalised to the integrated luminosity, as a function of $\alpha_{W\Phi}$, α_W and $\alpha_{B\Phi}$. The total number of selected events, hadronic and semileptonic, in the data (88) is also indicated in the figure. The distributions of $\cos\theta$ for semileptonic and hadronic events are shown Fig. 4. The data is well reproduced by the SM MC simulation.

Results for $\alpha_{W\Phi}$, α_W and $\alpha_{B\Phi}$ from semileptonic and hadronic events using the fits to the optimal observables are listed in Table 3. The distributions of the optimal observables can be found in Fig. 5. The MC distributions for different values of the couplings are also shown, illustrating the sensitivity to the TGCs. The final results from the combined fits for $\alpha_{W\Phi}$, α_W and $\alpha_{B\Phi}$, respectively, are also summarised in Table 3. The resulting negative $2\ln\mathcal{L}$ curves are shown in Fig. 6 for the three TGCs.

The 68% and 95% confidence intervals are obtained by integration of the likelihood functions due to the non-parabolic form of the negative $2\ln\mathcal{L}$ curves, which is most

Table 3: *The final results for $\alpha_{W\Phi}$, α_W and $\alpha_{B\Phi}$, from fits to the semileptonic and hadronic channels and the combined fit. The systematic uncertainties are shown in brackets.*

	Semileptonic	Hadronic	Combined	Combined 95% CL
$\alpha_{W\Phi}$	$-0.29^{+0.30(0.09)}_{-0.28(0.10)}$	$0.38^{+0.40(0.15)}_{-0.51(0.22)}$	$-0.14^{+0.27(0.14)}_{-0.25(0.12)}$	$[-0.64, 0.44]$
α_W	$-0.31^{+0.60(0.18)}_{-0.53(0.10)}$	$0.96^{+0.60(0.38)}_{-0.88(1.05)}$	$0.06^{+0.56(0.12)}_{-0.50(0.20)}$	$[-0.88, 1.13]$
$\alpha_{B\Phi}$	$-1.19^{+2.99(0.60)}_{-0.70(0.56)}$	$0.94^{+1.26(0.29)}_{-1.42(0.48)}$	$1.01^{+0.71(0.33)}_{-1.75(0.33)}$	$[-1.74, 2.41]$

pronounced for $\alpha_{B\Phi}$. The corresponding 95% confidence intervals from the combined fits are listed in Table 3. The systematic uncertainties for the 95% confidence intervals were estimated by scaling the studied effects. For the effects of jet algorithms or MC generators this procedure is not possible and the induced deviations were used.

Other experiments have measured the TGCs $\alpha_{W\Phi}$, α_W and $\alpha_{B\Phi}$ with comparable results [25, 26].

6   Conclusion

A measurement of triple gauge-boson couplings is presented in the semileptonic ($e\nu q\bar{q}$ and $\mu\nu q\bar{q}$) and hadronic decay modes in W pair production, based on a data sample collected by the ALEPH detector at a centre of mass energy of 172.086 GeV, corresponding to an integrated luminosity of 10.65 pb^{-1}.

The analysis includes full kinematic information and takes detector effects and background into account. The triple gauge-boson couplings are extracted by using likelihood estimation based on one-dimensional distributions of optimal observables, constructed from the four-fermion differential cross section.

Single parameter fits to the combined semileptonic and hadronic analyses for the three models, W_ϕ, W and B_ϕ, yielded 95% confidence levels

$$-0.64 < \alpha_{W\Phi} < 0.44$$
$$-0.88 < \alpha_W < 1.13$$
$$-1.74 < \alpha_{B\Phi} < 2.41,$$

in agreement with the Standard Model prediction. The separate results in both the hadronic and semileptonic channels are also consistent with the SM predictions. The systematic uncertainties are dominated by the choice of the jet reconstruction algorithm and colour reconnection, followed by the effects of using different MC samples to check the hadronisation and radiative corrections. However, the uncertainties are still largely dominated by the statistical precision of the data samples.

7   Acknowledgements

A   Semileptonic Neural Network Input Variables

The Neural Network (NN) calculates an approximation of the multidimensional probability density function in the following 25 input variables, for signal and backgrounds [27]. The NN is applied, after preselection, to events with at least one identified lepton with momentum – after bremsstrahlung correction for electrons – in excess of 17 GeV. In cases where there are more than one lepton candidate, the probability densities are calculated for each one, and the highest probability is kept for each hypothesis, signal and background. The NN uses variables related to the lepton candidate, to the missing momentum, global event variables, and WW kinematics. They are listed here together with their relative discriminating power, namely the statistical correlation with the neural network output.

   Lepton related variables:
– Lepton identification flag: 1 for electron, 2 for muon; (7.2%)
– Number of selected muons in the event; (5.6%)
– Number of selected electrons in the event; (4.2%)
– Lepton isolation: energy of charged tracks within a cone of 10 degrees around the lepton candidate; (5.6%)
– Lepton isolation: angle between the lepton candidate and the nearest charged track; (5.2%)
– Lepton isolation: energy of the nearest charged track; (2.3%)
– Lepton momentum: track momentum; (3.0%)
– Lepton momentum: track longitudinal momentum along the beam axis; (4.2%)
– Lepton momentum: track transverse momentum w.r.t. the beam axis; (4.8%)
– Momentum corrected for bremsstrahlung; (4.5%)
– Number of photons found by the bremsstrahlung correction; (2.0%)
– Total energy of all photons found by the bremsstrahlung correction; (1.8%).
   Global event variables:
– Number of good charged tracks in the event; (3.7%)
– Number of tracks with momentum greater than $0.1\sqrt{s}$; (2.1%)
   Missing Momentum Variables:
– Missing momentum; (4.7%)
– Missing transverse momentum; (8.9%)
– Missing energy; (3.5%)
– $|P^z_{\mathrm{miss}} + E_{\mathrm{miss}}/2|$, effective against $\tau\nu q\bar{q}$ events; (5.8%)
   WW Kinematics:
– Energy of the hadronically decaying W;(3.2%)
– Cosine of the angle between the lepton candidate and the production plane; (2.4%)
– Cosine of the angle between the lepton candidate and the plane defined by the vector $P_{\mathrm{lepton}} - P_{\mathrm{miss}}$ and the beam axis; (3.6%)
– Cosine of the angle between the lepton candidate and the missing momentum vector; (3.6%)
– Cosine of the angle between the missing momentum and the track most anti-parallel to it; (3.1%)
– Flag if the lepton is the track most anti-parallel to the missing momentum; (2.9%)
– Angle between the lepton candidate and the track most anti-parallel to the missing momentum; (2.4%)

B Hadronic Neural Network Input Variables

The Neural Network (NN) hadronic event selection uses 21 variables. The variables are related to i) global event properties, ii) flavour tagging to reduce the background from QCD events containing b quarks; iii) properties of jets; and iv) kinematic variables. The variables are listed below, together with their discriminating power.

Global event properties:
– Total visible energy in the event; (4.7%)
– Sum of momenta of all charged tracks in the event; (2.6%)
– Aplanarity; (4.7%)
– Oblateness; (3.8%)
– Fox-Wolfram moment H0; (3.8%)
– Fox-Wolfram moment H2; (5.4%)
– Fox-Wolfram moment H3; (7.0%)
– Fox-Wolfram moment H4; (6.8%)

Heavy Flavour tagging:
The b-tag probability of an ensemble of charged tracks is the product of the probabilities that each track comes from the primary vertex [28]. (b-jets have small probabilities).
– Sum of the b-tag probabilities for the four jets; (4.8%)
– Sum of logarithms of the b-tag probabilities for the four jets; (4.5%)
– Global b-tag probability, constructed from all charged tracks in the event; (2.6%)

Properties of Jets:
– Number of energy flow objects in the most energetic jet; (5.4%)
– Number of energy flow objects in the least energetic jet; (3.6%)
– Largest energy fraction carried by one energy flow object in the most energetic jet; (3.8%)
– Largest energy fraction carried by one energy flow object in the second most energetic jet; (4.8%)
– Largest energy fraction carried by one energy flow object in the third most energetic jet; (3.9%)
– Largest energy fraction carried by one charged track in the most energetic jet; (3.5%)

WW Kinematics:
– Sum of the cosines of the six angles between the jets; (9.2%)
– Largest of the smallest di-jet invariant masses from each of the three possible pairings; (6.1%)
– Largest invariant mass of all six di-jet combinations; (5.8%)
– Transverse momentum of the highest energy jet; (3.7%)

References

[1] T. Yasuda, "Tevatron results on Gauge Boson Couplings", FERMILAB CONF-97/206-E, to appear in proceedings of the the International Europhysics Conference on High-Energy Physics, Jerusalem (1997).

[2] K. Hagiwara, R. Peccei, D. Zeppenfeld and K. Hikasa, *Nucl. Phys.* **B 282** (1987) 253.

[3] G. Gounaris, J.-L. Kneur and D. Zeppenfeld, from "Physics at LEP2", CERN 96-01 p. 525, editors G. Altarelli, T. Sjöstrand and F. Zwirner.

[4] A.B. Lahanas and V.C. Spanos, *Phys. Lett.* **B 334** (1994) 378 (hep-ph/9504340);
E.N. Argyres, A.B. Lahanas, C.G. Papadopoulos and V.C. Spanos, UA/NPPS-18B (1995);
A. Arhrib, J.-L. Kneur and G. Moultaka, CERN-TH/95-344 (hep-ph/9512437).

[5] A. De Rújula, M.B. Gavela, O. Pène and F.J. Vegas, *Nucl. Phys.* **B357** (1991) 311.

[6] M. Bilenky, J.L. Kneur, F.M. Renard and D. Schildknecht, *Nucl. Phys.* **B409** (1993) 22.

[7] G. Gounaris, J. Layssac, G. Moultaka and F.M. Renard, *Int. J. Mod. Phys.* **A8** (1993) 3285.

[8] A. De Rújula, M.B. Gavela, P. Hernandez and E. Massó, *Nucl. Phys.* **B384** (1992) 3.

[9] ALEPH Collaboration, "ALEPH: A Detector for Electron-Positron Annihilations at LEP", *Nucl. Instr. Meth.* **A 294** (1990) 121.

[10] ALEPH Collaboration, "Performance of the ALEPH Detector at LEP", *Nucl. Instr. Meth.* **A 360** (1995) 481.

[11] M. Skrzypek, S. Jadach, W. Placzek and Z. Was, *Computer Phys. Comm.* **94** (1996) 216.

[12] F.A. Berends, R. Pittau and R. Kleiss, *Nucl. Phys.* **B 424** (1994) 308.

[13] T. Sjöstrand, *Computer Phys. Comm.* **82** (1994) 74.

[14] T. Sjöstrand and A. Khoze, *Phys. Rev.* **72** (1994) 28.

[15] ALEPH Collaboration, "An Experimental Study of $\gamma\gamma \rightarrow$ Hadrons at LEP", *Phys. Lett.* **B313** (1993) 509.

[16] G. Marchesini *et al.*, *Computer Phys. Comm.* **67** (1992) 465.

[17] ALEPH Collaboration, "Measurement of Mean Lifetime and Branching Fractions of b Hadrons Decaying to J/ψ", *Phys. Lett.* **B 295** (1992) 396.

[18] Yu.L. Dokshitzer, *J. Phys. G.* **17** (1991) 1441.

[19] JADE Collaboration, "Experimental Studies on Multi-jet Production in e^+e^- Annihilation at PETRA Energies", *Zeit. Phys.* **C33** (1986) 23; "Experimental Investigation of the Energy Dependence of the Strong Coupling Strength", *Phys. Lett.* **B213** (1988) 235.

[20] M. Diehl and O. Nachtmann, *Zeit. Phys.* **C62** (1994) 397.

[21] M. Rijssenbeck,"W mass from the Tevatron", FERMILAB CONF-96/365-E, Proceedings of the 28th International Conference on High Energy Physics, Warsaw (1996).

[22] S. Jadach and K. Zalewski, CERN-TH/97-27.

[23] F.A. Berends, G. Burgers and W.L. Van Neerven, *Phys. Lett.* **B185** (1987) 395; *Nucl. Phys.* **B297** (1988) 429; **B304** (1988) 921.

[24] Working group on LEP energy, private communication.

[25] L3 Collaboration, "Measurements of Mass, Width and Gauge couplings of the W Boson at LEP" , submitted to *Phys. Lett. B*, CERN-PPE-97-98.

[26] OPAL Collaboration, "Measurement of triple gauge boson couplings from W^+W^- production at $\sqrt{s} = 172$ GeV", submitted to *Z. Phys.*, CERN-PPE-97-125.

[27] C. Guicheney, "Développement de la technique des Réseaux de Neurones en physique des particules", PHD thesis, Université de Clermont-Ferrant, 1997.

[28] ALEPH Collaboration, "A Precise Measurement of $\Gamma_Z \to b\bar{b}/\Gamma_Z \to hadrons$", *Phys. Lett.* **B 313** (1993) 535.
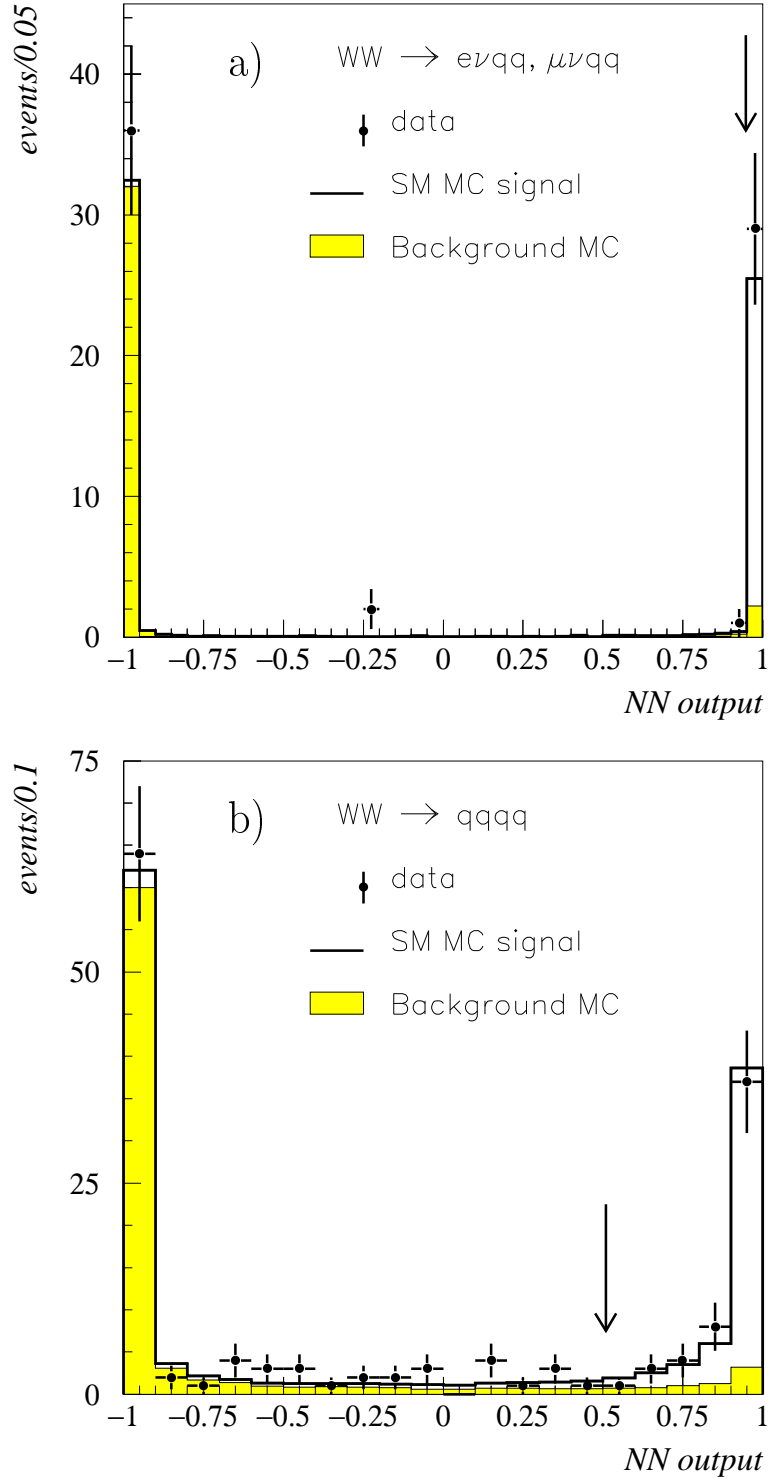
ALEPH

Figure 1: *The distributions of the neural network outputs for MC simulation and data. a) The distribution of the semileptonic neural network output. b) The distribution of the output from the neural network used in the hadronic event selection. The data is represented by the points with error bars and the MC simulation by the histograms. The solid histograms show the expected signal in data and the shaded areas show the expected distribution for background events from MC. The number of MC events is normalised to the integrated luminosity of the data. The arrow on each plot indicates the cut applied in the event selection.*
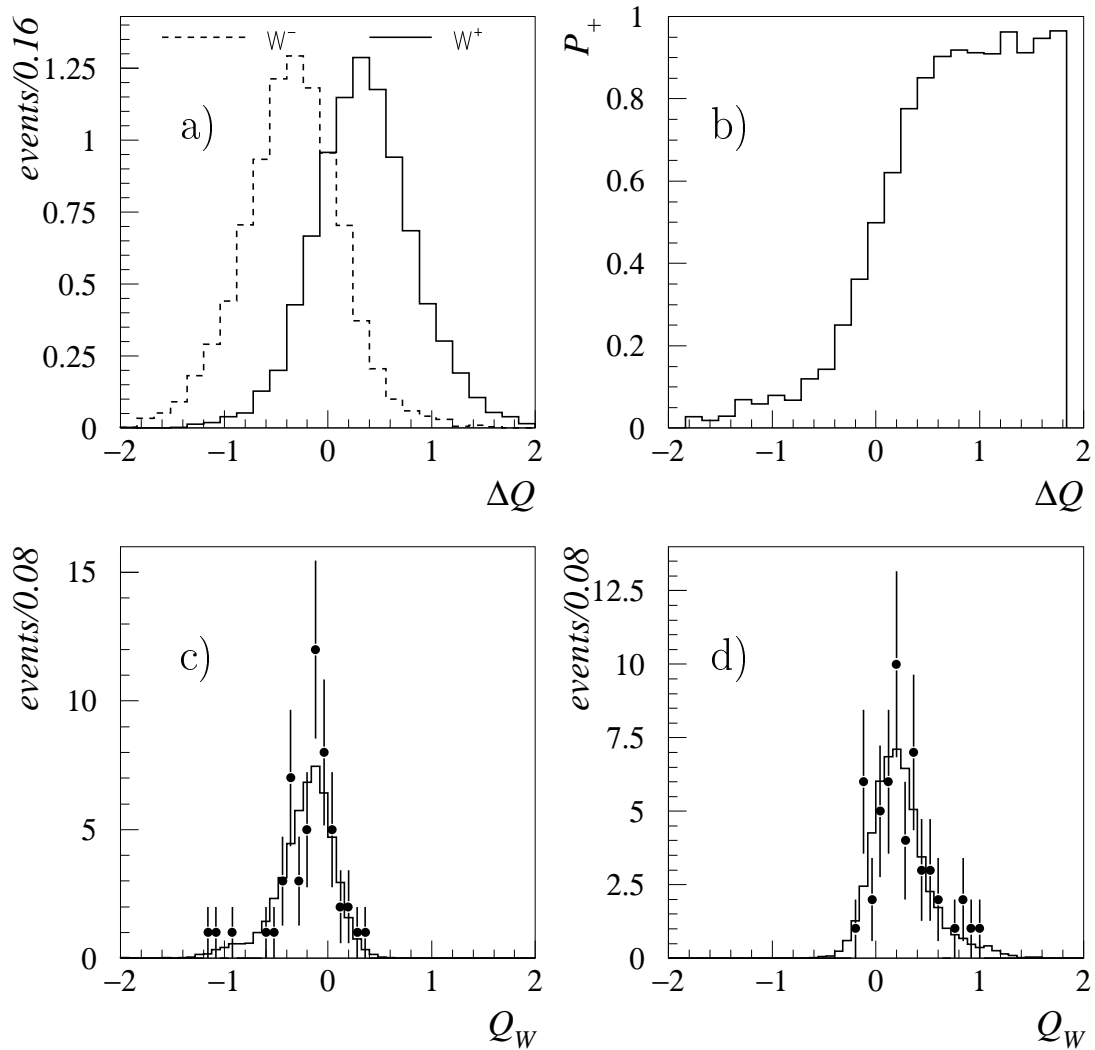
ALEPH

Figure 2: *W charge tagging distributions. a) The distribution of the charge difference for true W^+ (solid histogram) and true W^- (dashed histogram) decays for MC events. The true W^+ and W^- decays are identified in the MC using generator level information. b) The probability P_+ as function of the charge difference between the two W's. c,d) Experimental distributions of W^- (selected by $P_+ < 0.5$) and W^+ (selected by $P_+ > 0.5$) reconstructed charges, respectively. The data are represented by the dots and the MC simulation by the histograms. The number of MC events is normalised to the integrated luminosity of data.*
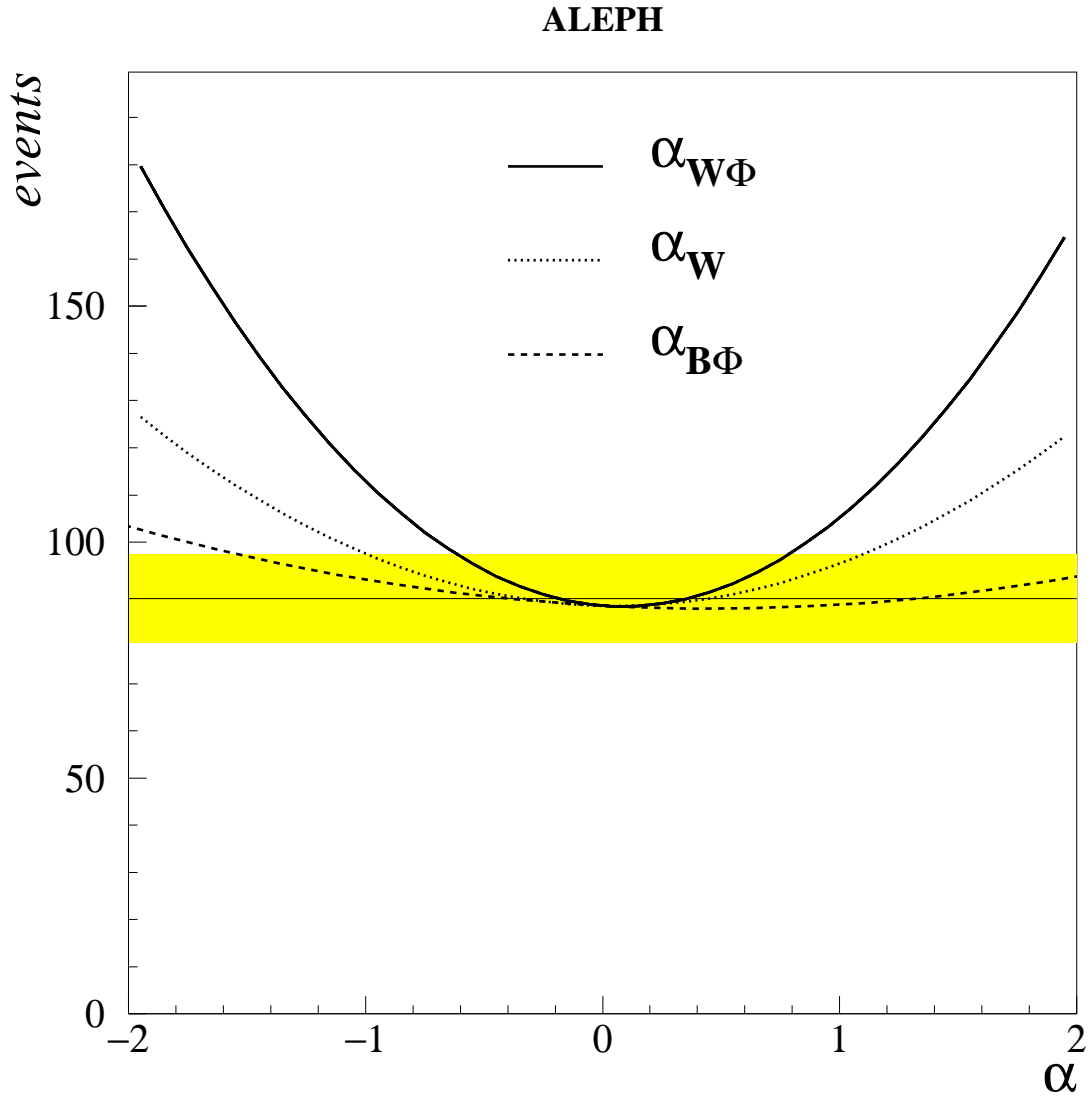
ALEPH

Figure 3: *The number of expected events as function of the couplings as indicated in the plot. The curve for each TGC is obtained under the assumption that the two other TGCs are fixed at zero, their Standard Model value. The total number of observed events, semileptonic and hadronic, is represented by the horizontal line and the corresponding statistical uncertainty is indicated by the band.*
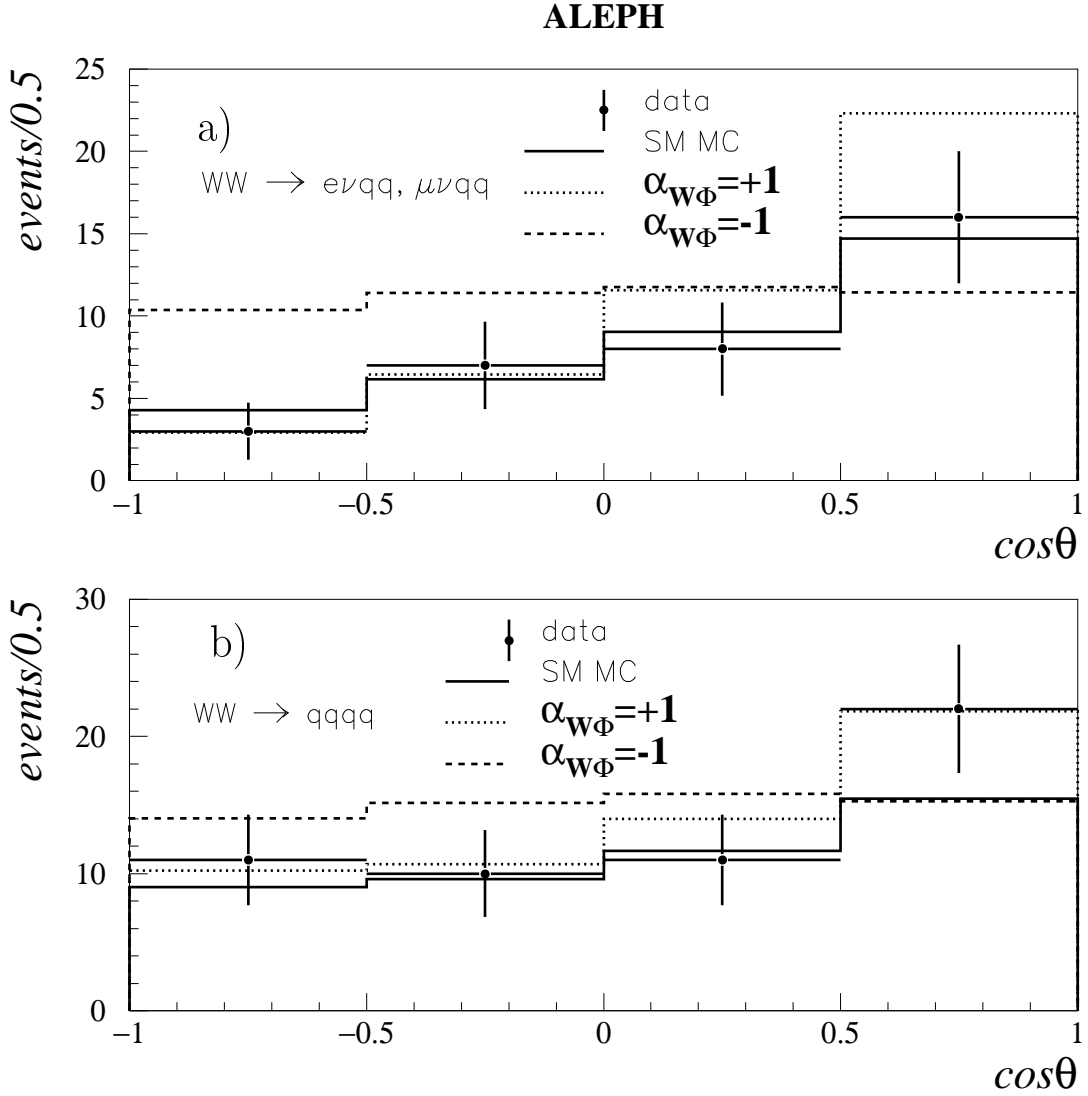
Figure 4: *The distribution of the cosine of the W^- production angle for various values of the coupling $\alpha_{W\Phi}$, for a) semileptonic and b) hadronic channels. The data is represented by the points with error bars and the MC simulation by the histograms. The solid histograms represent the Standard Model expectation, while the dashed and dotted histograms show the distributions for values of $\alpha_{W\Phi} = -1$ and 1, respectively.*
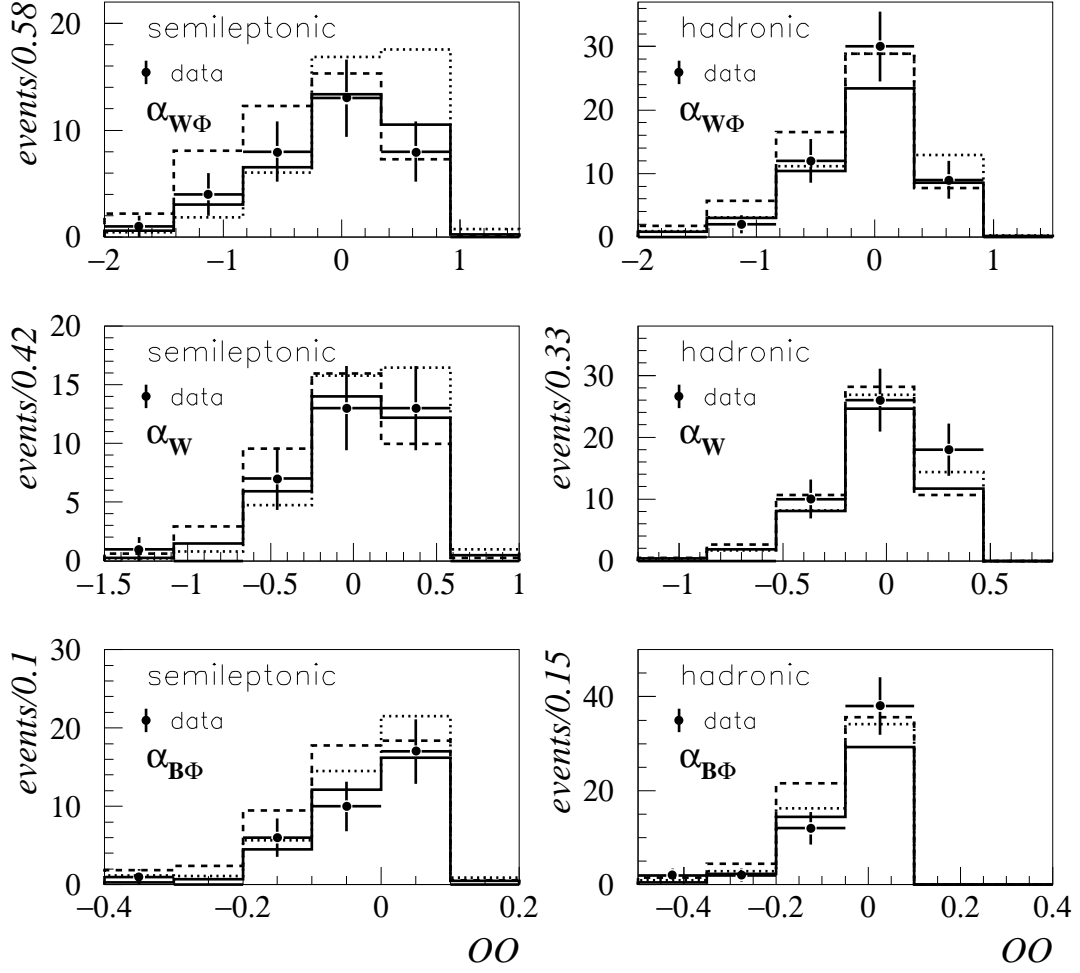
ALEPH

Figure 5: *The distribution of the optimal observable for various values of the couplings* $\alpha_{W\Phi}$, α_W *and* $\alpha_{B\Phi}$ *for semileptonic and hadronic channels. The data are represented by the solid dots and the MC simulation by the histograms. The solid histograms represent the Standard Model expectation. The dashed and dotted histograms show the distributions for values of the couplings* -1 *and* 1, *respectively. For* $\alpha_{B\Phi}$ *the corresponding histograms represent values of* $\alpha_{B\Phi} = -3$ *and* 3.
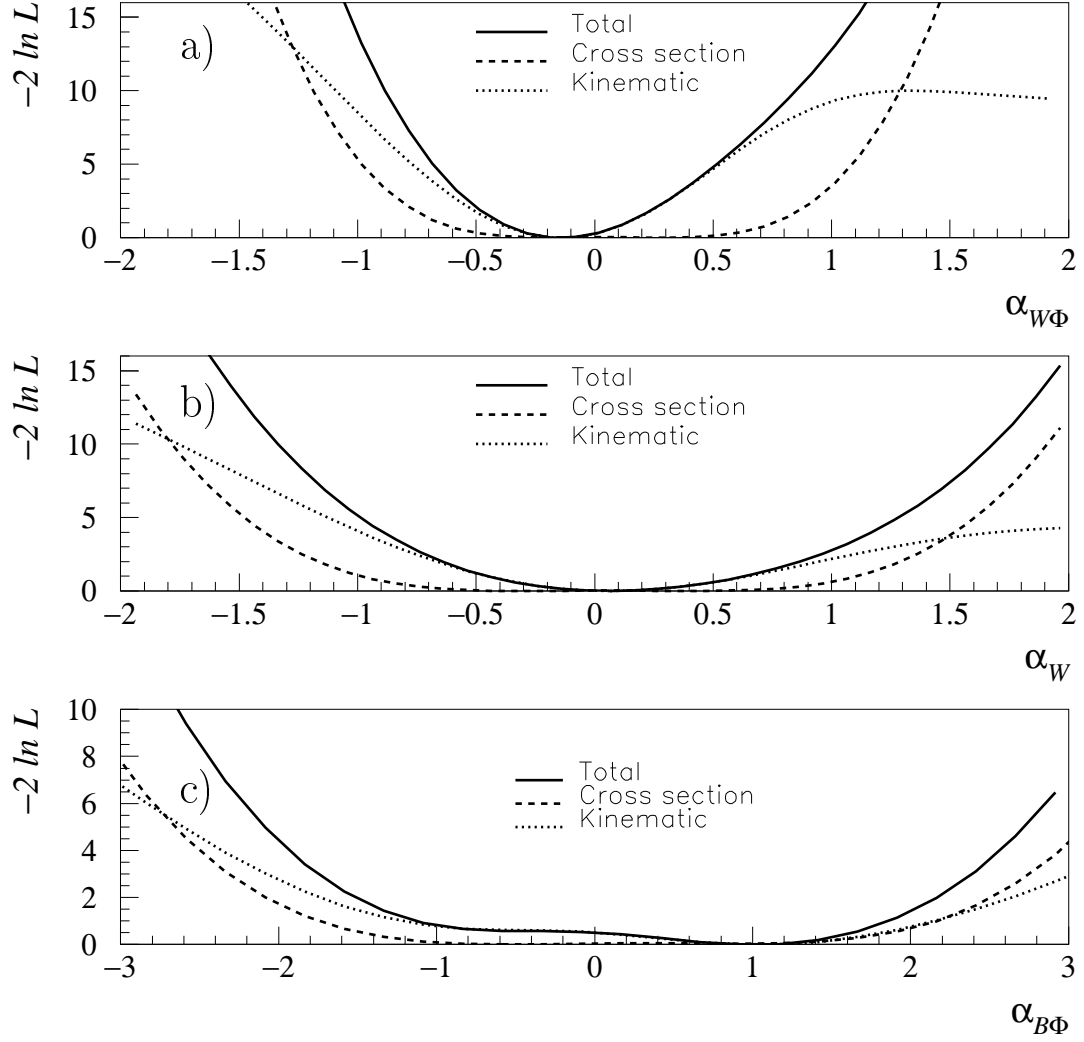
ALEPH

Figure 6: *The quantity* $-2\ln\mathcal{L}$ *for the combined fit to both semileptonic and hadronic channels for the three couplings* $\alpha_{\mathrm{W}\Phi}$, α_{W} *and* $\alpha_{\mathrm{B}\Phi}$. *The contributions of the cross section (dashed curve) and kinematic information (dotted curve) are also shown. a) The curves for* $\alpha_{\mathrm{W}\Phi}$. *b) The curves for* α_{W}. *c) The curves for* $\alpha_{\mathrm{B}\Phi}$.